



Universiteit
Leiden
The Netherlands

Magnetism of a single atom

Otte, A.F.

Citation

Otte, A. F. (2008, March 19). *Magnetism of a single atom*. *Casimir PhD Series*. LION, AMC research group, Faculty of Science, Leiden University. Retrieved from <https://hdl.handle.net/1887/12660>

Version: Corrected Publisher's Version

License: [Licence agreement concerning inclusion of doctoral thesis in the Institutional Repository of the University of Leiden](#)

Downloaded from: <https://hdl.handle.net/1887/12660>

Note: To cite this publication please use the final published version (if applicable).

Chapter 5

Initial Results on Further Experiments

As we have seen in the previous chapters, the Cu₂N surface provides an excellent environment for doing experiments aimed at characterizing the interplay of atomic spins with their direct environment. Clearly we have only just begun exploring its full potential and further progress is currently being made rapidly. In the final chapter of this thesis some initial results of a few promising experiments will be presented.

5.1 Distance Dependence of Spin Interaction

We concluded chapter 4 with the observation that, although we can very well describe the coupling between the spins in the X_{vv}Co structures of section 4.3.2 with an empirical Heisenberg parameter J , we still have no idea of the actual nature of the coupling (other than that it is not just dipolar interaction and therefore must be somehow mediated by the surface). As a first attempt towards identifying the physics behind this interaction, it is useful to investigate the variation of the coupling strength as a function of the distance between the spins. For example in the case of RKKY interaction [85], where the exchange coupling is carried by the conduction electrons in a Fermi sea (such as the bulk copper below the Cu₂N), its strength is expected to show a damped oscillation:

$$J_{\text{RKKY}}(\mathbf{r}) \propto \frac{r \cos(k_F r) - \sin(k_F r)}{r^4}, \quad (5.1)$$

where \mathbf{r} is the vector separating the spins and k_F is the length of the Fermi wave vector in the direction of \mathbf{r} .

The possibilities for varying the separation on Cu₂N are quite limited. Repeated attempts to build dimers where the atoms are separated by only one vacancy site (3.6 Å distance) were all unsuccessful, probably due to instability of the structure, while a separation of three vacancies or more yields no observable

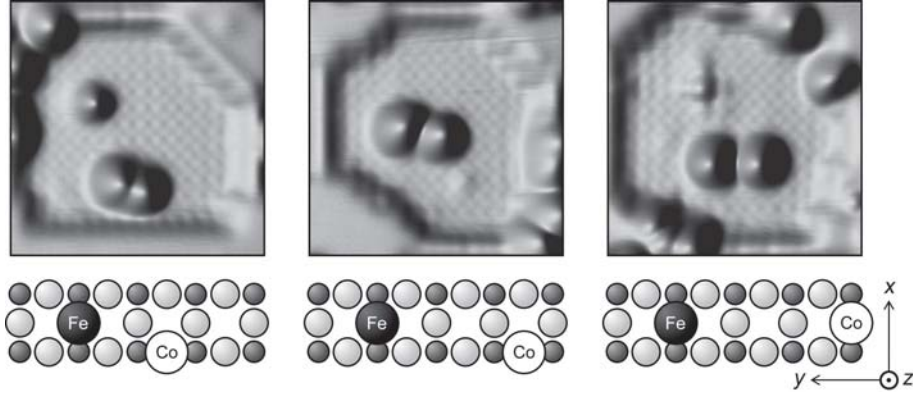


Figure 5.1: **Top row:** Topographic images (6×6 nm, 10 mV/1 nA) showing three Fe/Co dimers with different relative positions of the atoms; from left to right $\text{Fe}_{v\setminus}\text{Co}$, $\text{Fe}_{v\setminus\setminus}\text{Co}$ and Fe_{vv}Co . In each case the left atom is Fe, located on a horizontal v-row. In the left image the distance from the Co atom to the missing N-row that forms the edge of the island is 10.8 \AA (i.e. 3 unit cells). **Bottom row:** Corresponding drawings of the structure of the dimers where, as before, light circles indicate Cu atoms and small dark circles are N atoms. The assignment of the axes applies to all three structures.

coupling. In order to somewhat appropriately characterize the distance dependence of the interaction, dimers with orientations other than exactly along a v-row have to be included. Fig. 5.1 shows three variations on the Fe_{vv}Co structure¹, two of which have its Co atom lying off the v-row. Using the \setminus symbol to indicate a single diagonal step, we will refer to these objects as “ $\text{Fe}_{v\setminus}\text{Co}$ ” and “ $\text{Fe}_{v\setminus\setminus}\text{Co}$ ”, with direct separation distances of 5.7 and 9.2 \AA respectively. In the third, “ Fe_{vv}Co ”, the atoms are spaced by 10.8 \AA along the v-row.

On each of these structures dI/dV -spectra have been measured over the Co atom at various fields oriented in the x -direction. These should be compared to fig. 4.7b, showing equivalent measurements performed on Fe_{vv}Co : here we saw that the external field cancels the influence of the Fe spin around $B = 2$ T. Results for $\text{Fe}_{v\setminus}\text{Co}$ are shown in fig. 5.2a. Again the proximity of the Fe atom causes a splitting of the Kondo peak at zero field, but this time the ‘effective field’ is much stronger: the peaks seem to converge around 9 T. Also the spectra feature two steps at higher energy rather than only one. In the case of $\text{Fe}_{v\setminus\setminus}\text{Co}$ (fig. 5.2b) the effect of the coupling is much weaker such that no splitting can be observed at zero field.

When trying to model these two ‘semi-diagonal’ systems as we did in chapter 4 for Fe_{vv}Co , we should bear in mind that not only the relative positions, but also the relative orientations of the two spins have changed. Previously the Co spin (having its primary anisotropy axis \mathcal{Z} oriented locally along the v-row) had its hard-axis perpendicular to the Fe spin’s easy-axis (oriented along the N-

¹This combination is most suitable: Mn_{vv}Co has a much smaller J and the spectra of Co_{vv}Co are somewhat confusing due to its many low-energy excitations.

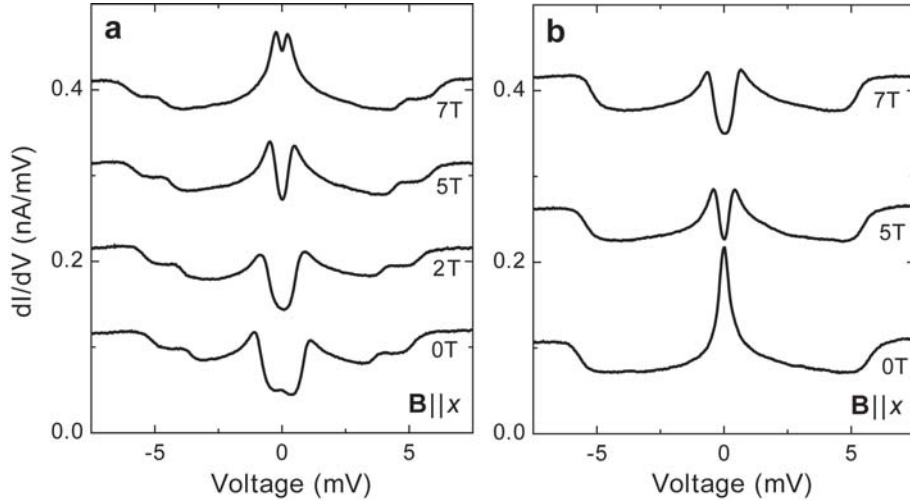


Figure 5.2: dI/dV -spectra measured over the Co atoms of Fe_v\Co (a) and Fe_{vv}\Co (b) at various fields with $\mathbf{B} \parallel x$. Curves obtained at non-zero fields are offset with 0.10 nA/mV in (a) and 0.15 nA/mV in (b).

row). However, in the current situations the local environment of the Co atom has rotated by 90° with respect to the Fe atom: both spins now have their primary anisotropy axis pointing in the x -direction. The proper Heisenberg model Hamiltonian thus becomes:

$$\begin{aligned} \hat{\mathcal{H}} = & J\hat{\mathbf{S}}^{(\text{Fe})} \cdot \hat{\mathbf{S}}^{(\text{Co})} - \mu_B \mathbf{B} \cdot (g_{\text{Fe}}\hat{\mathbf{S}}^{(\text{Fe})} + g_{\text{Co}}\hat{\mathbf{S}}^{(\text{Co})}) \\ & + D_{\text{Fe}}\hat{S}_x^{2(\text{Fe})} + E_{\text{Fe}}(\hat{S}_y^{2(\text{Fe})} - \hat{S}_z^{2(\text{Fe})}) + D_{\text{Co}}\hat{S}_x^{2(\text{Co})}, \end{aligned} \quad (5.2)$$

which differs from (4.20) only in the subscript of the very last term. Starting with Fe_v\Co, we see in fig. 5.3 that with a J -value of 0.48 ± 0.02 meV, (5.2) very well reproduces the measured peak positions, as well as both of the steps. So by reducing the spacing between the atoms by merely 20%, their interaction has become almost four times stronger (Fe_{vv}\Co has $J = 0.13$ meV). The appearance of the extra step around 4 mV is a direct consequence of this. If we express the two excited states corresponding to either step, $|\psi_5\rangle$ and $|\psi_7\rangle$, in the basis of $\hat{S}_x^{(\text{Fe})}$ and $\hat{S}_x^{(\text{Co})}$ eigenstates $|m_{\text{Fe}} m_{\text{Co}}\rangle$ at $B = 0$, we find:

$$\begin{aligned} |\psi_5\rangle = & -0.60|+2-\frac{3}{2}\rangle - 0.30|-1-\frac{1}{2}\rangle + 0.68|+1-\frac{1}{2}\rangle, \quad \text{and} \\ |\psi_7\rangle = & -0.77|+2-\frac{3}{2}\rangle + 0.44|-1-\frac{1}{2}\rangle - 0.39|+1-\frac{1}{2}\rangle, \end{aligned}$$

where other contributions up to 0.21 were neglected. Interestingly, the excitation to $|+2-\frac{3}{2}\rangle$ (from ground state $|+2-\frac{1}{2}\rangle$), which is expected to occur when the tip is placed over the Co atom, has strongly mixed with two excitations

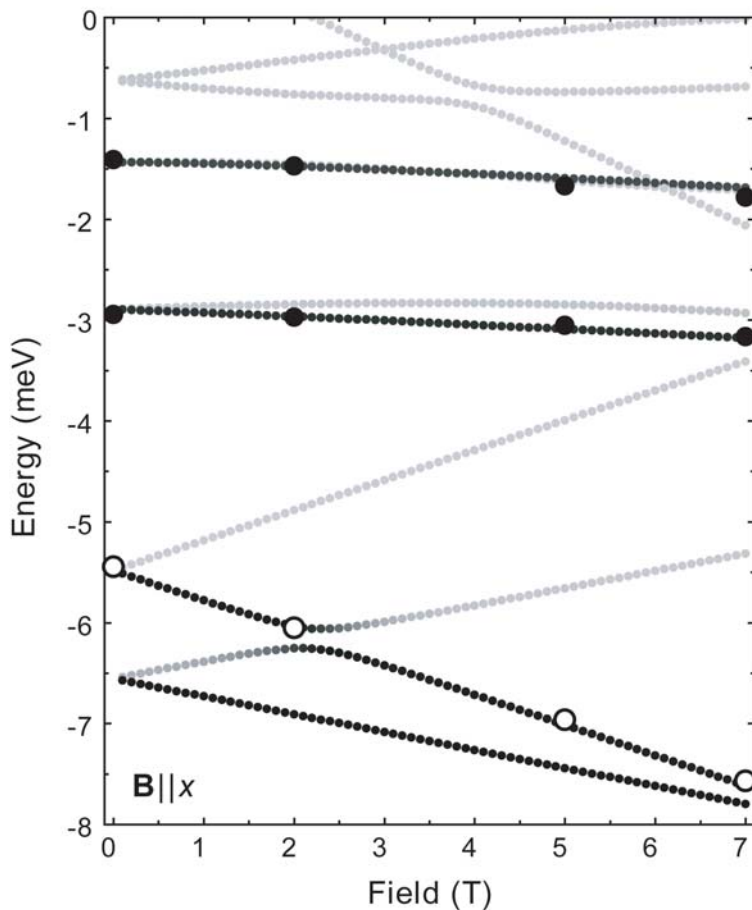


Figure 5.3: Lowest 11 eigenvalues of (5.2) with $J = 0.48$ meV, $g_{\text{Fe}} = 2.11$, $g_{\text{Co}} = 2.16$, $D_{\text{Fe}} = -1.55$ meV, $E_{\text{Fe}} = 0.31$ meV and $D_{\text{Co}} = 2.70$ meV for $\mathbf{B} \parallel x$. For each level $|\psi_n\rangle$ the corresponding transition intensity $I_{0 \rightarrow n}^{(\text{Co})}$, i.e. with the tip placed over the Co atom, is shown in greyscale (see fig. 5.4 for key and section 4.3.3 for an introduction into the representation used in this graph). Experimental data points extracted from fig. 5.2a.

of the Fe spin² and is now distributed over two transitions. This is an important result: apparently the two spins are now so strongly coupled that we can no longer make excitations on only one of them without influencing the other. Gradually the structure is becoming a single spectroscopic entity.

The longer semi-diagonal structure $\text{Fe}_{v,v} \setminus \text{Co}$ is more difficult to analyze properly, as we have only few data points on it and the energy resolution is insufficient to make out any zero-field splitting. However, due to the cal-

²Actually with only one Fe excitation: $|+1-\frac{1}{2}\rangle$. This one has in turn mixed with $|-1-\frac{1}{2}\rangle$ because of the finite value of E_{Fe} .

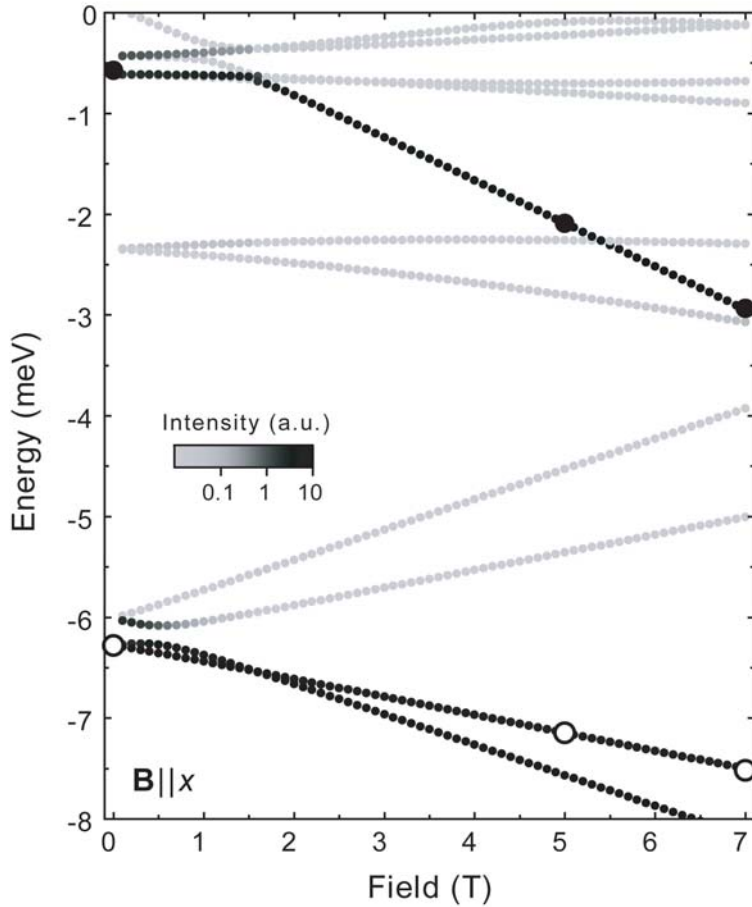


Figure 5.4: Lowest 11 eigenvalues of (5.2) with $J = 0.10$ meV, $g_{\text{Fe}} = 2.11$, $g_{\text{Co}} = 2.16$, $D_{\text{Fe}} = -1.55$ meV, $E_{\text{Fe}} = 0.31$ meV and $D_{\text{Co}} = 2.70$ meV for $\mathbf{B} \parallel x$. Experimental data extracted from fig. 5.2b. **Inset:** key for the greyscale representation of $I_{0 \rightarrow n}^{(\text{Co})}$.

culated higher-energy excitations evolving in a distinct nonlinear fashion we can extract a fitting value of J , albeit with a somewhat larger error margin: $J = 0.10 \pm 0.05$ meV. Figure 5.4 shows the corresponding energy level diagram.

Finally there is the 10.8 Å long $\text{Fe}_{\text{VVV}}\text{Co}$ structure. Spectra measured on its Co atom with $\mathbf{B} \parallel x$ (not shown here) look very similar to the results obtained on a free Co atom (i.e. fig. 4.4c). The only notable discrepancy – a slight downshift in energy for all excitations – indicates a marginally positive J , but might as well result from the usual 5% variations in the anisotropy parameters. It is best described with $J = 0.02 \pm 0.02$ meV.

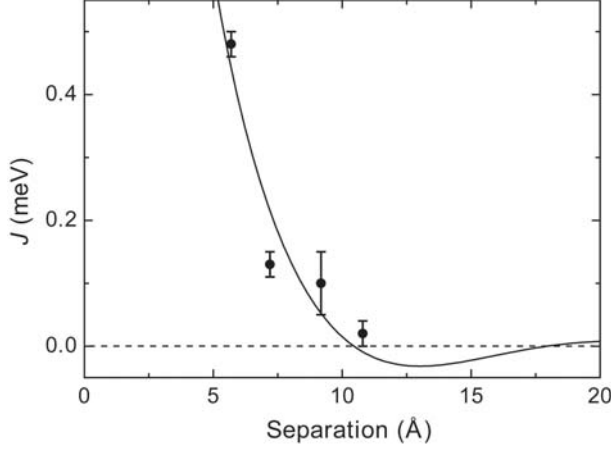


Figure 5.5: Plot of the experimentally determined values for J as a function of the direct separation distance between the atoms in various Fe/Co dimers on Cu_2N . The solid line shows a fit using (5.1) with $k_F = 0.43 \pm 0.06 \text{ \AA}^{-1}$.

We have now collected four data points characterizing the distance dependence of J , which are plotted in fig. 5.5. The measurements systematically indicate a very steep decline of the coupling strength. Several remarks should be made with respect to this graph. First, for the semi-diagonal structures we used the direct distance between the atoms, ignoring any possible anisotropies in the spin-interaction and in k_F arising from the Cu_2N lattice. In this context it is important to note that these structures are *not* invariant under switching the positions of the Fe and Co atoms, and were chosen arbitrarily. The inverted structures (e.g. $\text{Co}_v \setminus \text{Fe}$ instead of $\text{Fe}_v \setminus \text{Co}$) have not been investigated, but might give a different J at the same separation distance. Second, the available data points are still too few and too close to each other to make any claim concerning the nature of the coupling. The solid curve in fig. 5.5 only gives a best fit of J_{RKKY} , assuming that (5.1) is valid.

Having said that, the RKKY interaction proposed by the fit is certainly not unrealistic. It would explain the sharp increase of J below 7 \AA and the resulting value for the Fermi wave vector, $k_F = 0.43 \text{ \AA}^{-1}$, is reasonable. For comparison: in bulk copper (having the same lattice constant of 3.6 \AA) k_F varies along the Fermi surface from 1.36 to 1.51 \AA^{-1} . The reduction by a factor of ~ 3 may be caused by local deformations of the Fermi surface due to the loss of symmetry in Cu_2N , especially if that results in the creation of pockets of states at the Brillouin-zone boundary having lower effective wave vectors. Overall it is not unthinkable that with a few extra measurements in the range $r = 11 - 15 \text{ \AA}$ (e.g. $\text{Fe}_{vvv} \setminus \text{Co}$), where J is expected to become negative, the suggestion of RKKY interaction as presented can eventually be confirmed.

5.2 Coupling Along the N-Row

A different way of modifying the interaction between the atoms is to couple them along the N-direction rather than the v-direction. In contrast to previous work [19], where atoms were placed along an N-row at intervals of a single lattice spacing (3.6 Å), in this section we will focus on structures with 7.2 Å separation.

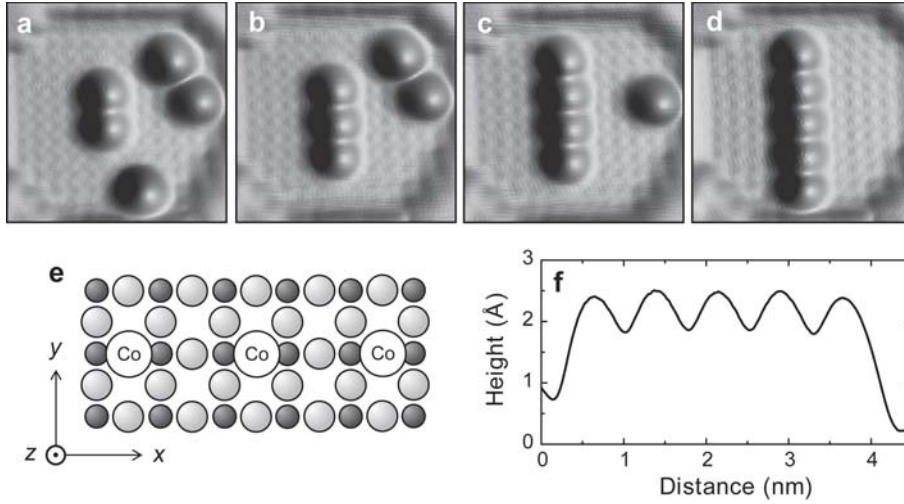


Figure 5.6: (a–d) Topographic images (5×5 nm, 10 mV/1 nA) of $\text{Co}(\text{NNCo})_{n-1}$ for $n = 2, 3, 4$ and 5 respectively. Comparable structures made of Fe have similar topographic appearances. (e) Structural drawing of $\text{Co}(\text{NNCo})_2$ with axis assignments. (f) Height profile extracted from (d) taken along the ridge of the structure (upward).

Figures 5.6a–d show topographic images recorded during the construction of a 28.8 Å long Co pentamer. To add a Co atom to the chain, it is first placed at the N site that is 9.0 Å away from the last atom of the chain, after which it is hopped in place (section 2.3.3). Although the atom can in principle hop two ways, the ‘success rate’ of the hopping procedure seems to increase with the length of the chain. As with the structures built along the v-rows at equal distance, atoms can be removed from the chain (both from the ends and from the center) without inflicting damage. We will refer to the subsequent structures shown in the figure as “ $\text{Co}(\text{NNCo})_{n-1}$ ” with n , the number of atoms in the chain, ranging from 2 to 5. Comparable structures were made with Fe instead of Co, having a very similar topographic appearance as their Co counterparts. In the following we will discuss spectroscopic results obtained on either class of structures, starting with $\text{Fe}(\text{NNFe})_{n-1}$.

5.2.1 The Ising Chain: Ferromagnetic Coupling?

Conductance spectra measured on all atoms of each of the four $\text{Fe}_{(\text{NNFe})_{n-1}}$ structures with $n \leq 5$ are shown in fig. 5.7, all at $B = 0$. The excitations in these cases appear at considerably higher energies than before (as a result of stronger coupling), such that the influence of a magnetic field would be much less prominent and will therefore not be considered here. What strikes immediately is that, except for a few details, there are only two kinds of spectra. Those measured over atoms located at either end of a structure (‘outer’ atoms) feature a single³ step around 7 mV, while the remaining spectra (taken over ‘inner’ atoms) have a step around 10 mV. It seems as if the excitation energies on each atom are determined only by the number of nearest neighbors: one or two respectively. The results can be modelled surprisingly well using a Hamiltonian based on Ising interaction combined with uniaxial anisotropy:

$$\hat{\mathcal{H}} = \sum_{i=1}^{n-1} J \hat{S}_x^{(i)} \hat{S}_x^{(i+1)} + \sum_{i=1}^n D \hat{S}_x^{2(i)}, \quad (5.3)$$

where J is the Ising interaction parameter and the operator $\hat{S}_x^{(i)}$ quantifies the x -component of the magnetization of the i -th spin in the chain. As before, D is the anisotropy parameter along x , the primary anisotropy axis for Fe.

Conveniently, this Hamiltonian is diagonal in the basis of all $\hat{S}_x^{(i)}$ eigenstates, expressed by the quantum numbers m_i , such that we can solve it analytically. Assuming D to be negative (as found for a single Fe atom), its ground state has $|m_i| = 2$ for all i , while the sign of J determines whether the spins have parallel or antiparallel alignment. One can easily demonstrate that in either situation a $|\Delta m_i| = 1$ transition on the spin of an outer atom will cost $2|J| - 3D$, while the same excitation on an inner spin costs $4|J| - 3D$. Combining this with the measured excitation energies we find $|J| \simeq 1.5$ meV and $D \simeq -1.3$ meV, which is not at all unreasonable (compared to $D = -1.55$ meV for single Fe). Within this model J can in principle have either sign, although based on what we have seen above it is unlikely to become negative.

The Ising Hamiltonian presented differs in two ways from the Heisenberg model we have successfully used so far. First, only the x -components of the spins are coupled rather than all components equally, and second, $E = 0$. Changing either of these two properties only slightly would sufficiently mix the eigenstates as to allow several additional excitations that are not observed. The sudden disappearance of E might be interpreted as a first observation of magnetic atoms significantly influencing each other’s local environment (although there is no particular reason for the coupling along x to lift the difference between the y and z -directions). Most intriguing, however, is the apparent change in the nature of the coupling mechanism: from fully isotropic to strongly directional.

³In case of the dimer, Fe_{NNFe} , the step actually consists of two smaller steps. We will ignore this for now.

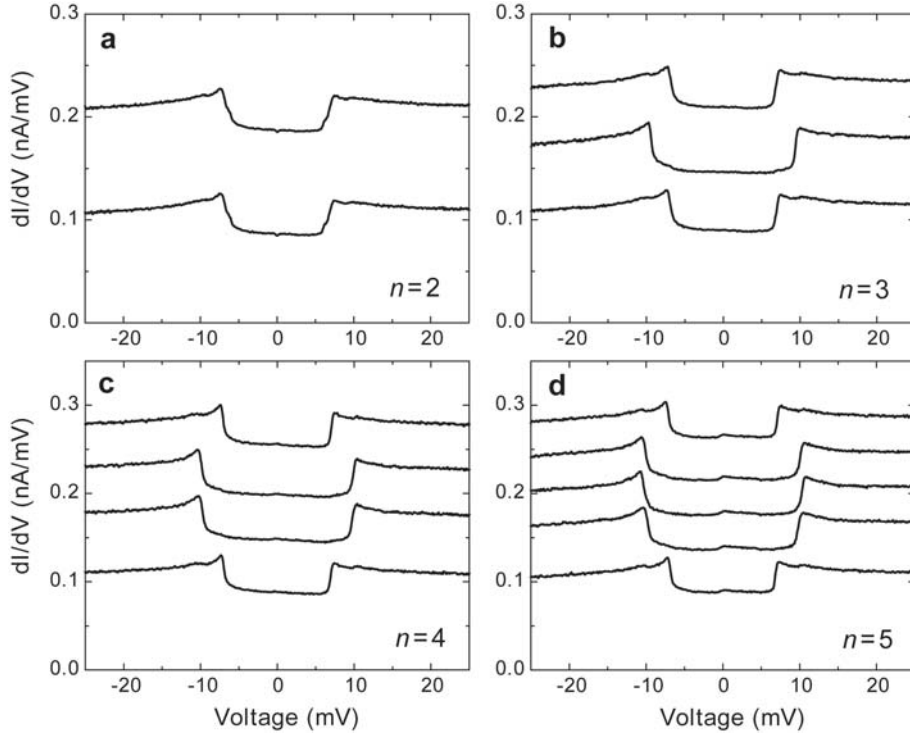


Figure 5.7: dI/dV -spectra measured over each of the Fe atoms in $\text{Fe}(\text{NNFe})_{n-1}$ structures with $n = 2, 3, 4$ and 5 . In each panel all curves except for the lowest are shifted upward by arbitrary amounts. The absolute conductance values are not relevant for the discussion presented here, but can be retrieved by considering that the integral of each spectrum up to 10 mV (quiescent voltage) should be equal. The vertical order corresponds to the positioning of the atoms within the structure (i.e. top and bottom curves were measured over the atoms on either end of the chain, etc.).

Interestingly, the results can be partly explained also *within* the framework of Heisenberg coupling by choosing J to be negative, i.e. by assuming ferromagnetic interaction. For instance in the case of the dimer ($n = 2$), the Heisenberg term does mix the $|m_1, m_2\rangle = |+2, -2\rangle$ and $|-2, +2\rangle$ states, but leaves $|+2, +2\rangle$ and $|-2, -2\rangle$ unchanged. This would justify the absence of a low-energy excitation, although additional excitations towards $|m_i| = 1$ states should still be expected.

Isn't the interpretation of ferromagnetic coupling inconsistent with the discussion on RKKY interaction of the previous section? After all, the separation distance is still 7.2 \AA which according to fig. 5.5 should result in a positive J . Yes, but that graph is based on coupling along the v-row, and its resulting value for k_F is significantly lower than expected based on the lattice constant (which is equal to the bulk copper lattice constant). Possibly the anisotropy of the Fermi surface of Cu_2N is such that along the N-row k_F is much closer to the

value for bulk copper. In that case, at a distance of two lattice spacings we could already have reached the first negative part of the RKKY oscillation. A similar study of the distance dependence of the coupling along the N-row may help verify this. For starters: at 3.6 Å separation along the N-row the interaction between Mn atoms was found to be antiferromagnetic ($J = 6.2$ meV) [19].

5.2.2 Closure of the Inelastic Channel

⁴ Even more challenging are the results obtained on the $\text{Co}_{(\text{NNCo})_{n-1}}$ structures as shown in fig. 5.8. First of all, not a single Kondo peak is observed in any of the spectra. Second, the results for $n = 2$ are dramatically different from those for $n \geq 3$, in which case there is again a sharp distinction between spectra taken on inner and on outer atoms. But the most surprising is that the spectra corresponding to inner atoms appear to be completely flat. Additional measurements on these atoms up to ± 100 mV did not show any feature, other than a gradual rise in the dI/dV for negative voltage and perhaps two very weak bumps around -10 mV and $+30$ mV.

The excitations measured on the dimer Co_{NNCo} can be modelled reasonably successfully using a $J \simeq 3.2$ meV Heisenberg model⁵, but this is certainly not the case for any of the other spectra. Regardless of what values are chosen for all the spin parameters, there should always be at least one excitation having a large enough transition intensity based on (3.4) to be observed. So it seems like the excitations themselves are still possible, but that they cannot be accessed for a different reason.

It is important to observe that even on the inner atoms the elastic part of the conductance is still fully intact. This can be derived from fig. 5.6f showing the height profile of $\text{Co}_{(\text{NNCo})_4}$ taken at 10 mV: if the elastic conductance would have been suppressed, the three inner atoms would have appeared significantly smaller in topography. This means that whatever process is responsible for disabling the spin excitations, is selective and only applies to the inelastic conductance. Let us therefore look more closely into the mechanism of inelastic spin excitation. On a Co atom, the net spin is carried by the 7 electrons in the 3*d*-states which are localized relatively closely around the nucleus, while most elastic conductance is expected to pass through the more widely spread *s* and *p*-states. In order to make an inelastic spin excitation, conduction electrons from the tip may have to tunnel into one of the five 3*d*-states. Of these only $3d_{z^2}$ has a finite electron density straight above the atom, where as usual we choose *z* to be oriented perpendicular to the sample-surface. The others (i.e. $3d_{xy}$, $3d_{xz}$, $3d_{yz}$ and $3d_{x^2-y^2}$) all have nodes along the *z*-axis.

⁴The interpretation presented in this section was based on discussions with J. van den Brink and J. van Wezel.

⁵Choosing $D = -2.3$ meV and $E = 0.6$ meV reconstructs the energies of all four excitations as well as much of their relative intensities. Interestingly, the system appears to have changed from hard-axis anisotropy along *y* for single Co into a configuration with an easy-axis (presumably perpendicular to *y*). This might explain the sudden absence of Kondo behavior (see section 4.2.2). However, as these findings are not too relevant for the discussion in this section, they will not be presented in more detail.

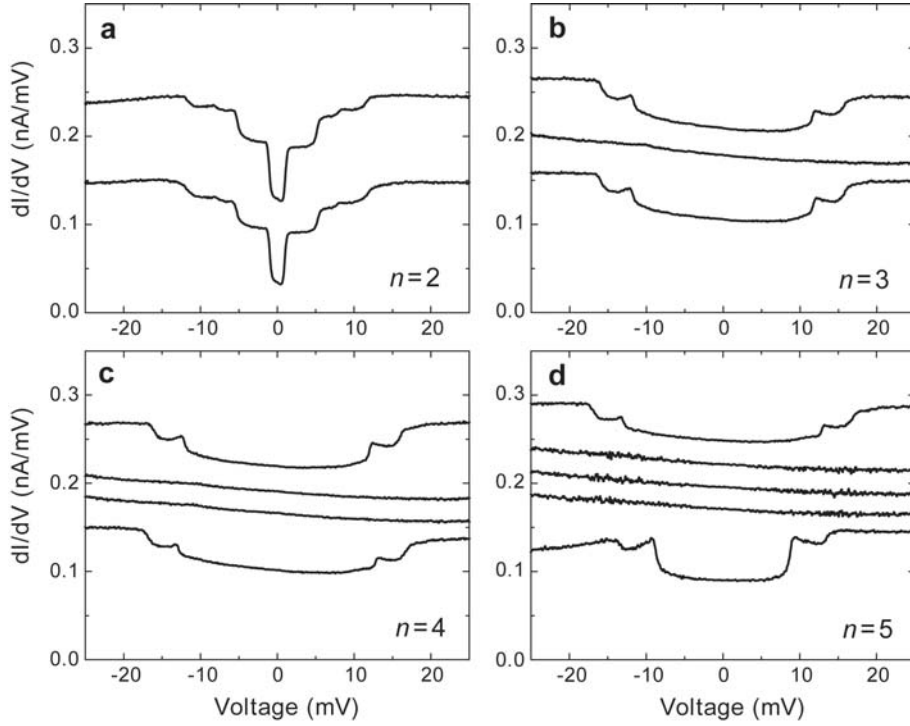


Figure 5.8: dI/dV -spectra measured over each of the Co atoms in $\text{Co}(\text{NNCo})_{n-1}$ structures with $n = 2, 3, 4$ and 5 ($10 \text{ mV}/1 \text{ nA}$ quiescent). In each panel all curves except for the lowest are shifted upward by arbitrary amounts. As before, the vertical order corresponds to the positioning of the atoms within the structure.

In this context the suppression of the excitations could – by way of speculation – be interpreted as a rearrangement of the $3d$ -orbitals due to spin coupling causing the $3d_{z^2}$ -state to shift away from the Fermi energy, thus becoming inaccessible for conduction electrons. Another way of looking at this is that the orbitals have rotated such that there no longer is a $3d_{z^2}$ -state (having been replaced by e.g. $3d_{x^2}$): now all orbitals have a node along z . None of this happens on the outer atoms as these are coupled to only one neighbor, leading to a different rearrangement of the orbitals. An obvious experiment to test this hypothesis would be to do spectroscopy while the tip is displaced horizontally with respect to the atom. Due to our automated atom-locking procedure (section 2.3.1), all present measurements were performed straight above the atom. If proven correct, this insight tells us that the $3d$ -orbitals play a prominent role in, or are at least strongly influenced by, the process of spin-spin coupling.

In the inner spectra of $\text{Co}(\text{NNCo})_4$ (fig. 5.8d) a remarkable noise is observed between 10 and 20 mV , symmetric around zero voltage. It is possible that this is somehow related to the excitations that are (supposedly) suppressed, although one can only speculate as to what mechanism is behind this.

5.3 Single-Atom Spin Filter

The art of filtering tunneling electrons based on their magnetic polarization was experimentally realized first by means of a ferromagnetic, or ferromagnetically coated tip [13]. This tool greatly expanded the scope of STM by making the magnetic structure of various surfaces directly visible [86, 87]. Further improvement to the technique was made through the introduction of antiferromagnetic tips [14], which strongly reduced the disturbing influence of the probe's dipolar stray field. In this section we will discuss an initial attempt towards the creation of the ultimate spin filter: a single magnetic atom attached to the apex of a non-magnetic tip.

Figure 5.9 shows the influence of a Co atom at the apex of the tip on its spectroscopic qualities. For this experiment a tip was formed (by repeated poking) that could reliably pick up and drop off atoms (section 2.3.3), each time reproducing the same atomic-scale tip geometry as seen from topography. With the tip in its 'empty' state a Cu atom (that could be identified as such

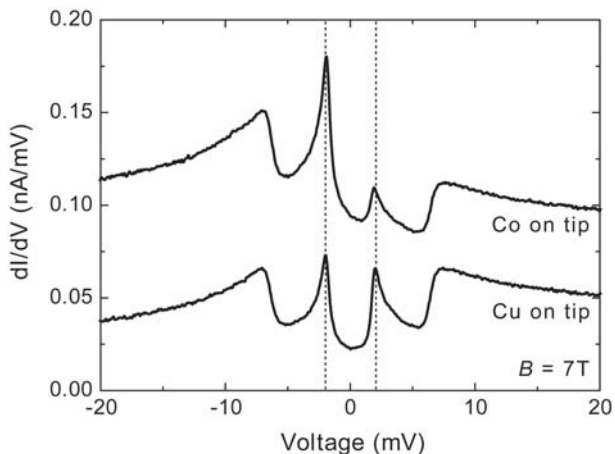


Figure 5.9: dI/dV -spectra taken over the same Co atom both before (lower curve) and after (upper curve) the Cu atom at the tip apex was replaced by a Co atom, at $B = 7$ T oriented out-of-plane. The lower spectrum was shifted down by 0.05 nA/mV.

through methods described in chapter 2) was picked up after which a standard spectrum at $B = 7$ T was taken over a Co atom, resulting in the lower curve. Next the Cu atom was replaced by a Co atom, with which the upper spectrum was taken over the same Co atom as before. The effect is striking: whereas for the neutral tip the two resonance peaks are equally high, with the magnetic tip the ratio of their heights is almost 4 : 1, while their position is not affected.

Although clearly the symmetry between the two spin polarizations is somehow broken, it is not easy to find a solid explanation for this phenomenon. It is tempting to say that if only electrons with one polarization (say \downarrow) are available

at the tip, these can tunnel into only one of the two resonances of the Kondo system. But as we have seen in section 4.3, the distinction between the two peaks is not at all made by spin polarization (\uparrow vs \downarrow), but by the fact that one belongs to the electron DOS and the other to the hole DOS. In each of the two resonances the localized spin continuously flips between either of the two excited states: \uparrow (with an electron-hole pair in the Fermi sea) and \downarrow (with the Fermi sea unexcited). Seeing that the ground state is \uparrow with an unexcited Fermi sea, arguably only the second of these excitations is directly accessible for electrons tunneling from the tip into the localized spin. Assuming that this can only be done by \downarrow electrons, the electron-hole symmetry might be broken in the case of a spin-selective tip.

A few points worth mentioning are that (1) the regular excitation steps in fig. 5.9 do not seem to be influenced too much by the magnetic tip (these are the excitations to $m = \pm\frac{3}{2}$) and that (2) the asymmetry of the peaks appears to be independent of field strength. Even at 2 T, the smallest field where the two peaks can still be discerned (not shown), the height ratio is close to 4 : 1.

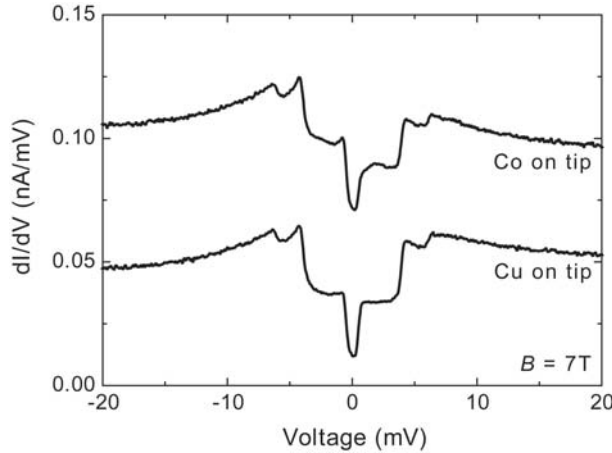


Figure 5.10: dI/dV -spectra taken over the same Fe atom both before (lower curve) and after (upper curve) the Cu atom at the tip apex was replaced by a Co atom, at $B = 7$ T oriented out-of-plane. The lower spectrum was shifted down by 0.05 nA/mV.

Interestingly, when doing the same experiment over an Fe atom as shown in fig. 5.10, the inner steps (between $|m| = 2$ states, see section 3.3.2) do become asymmetric, while those around 5 mV ($|m| = 2 \rightarrow 1$) seem to be unaltered. This is not at all surprising in view of that fact that the $|m| = 1$ states are mixed much stronger by the transverse anisotropy parameter E than those with $|m| = 2$, and have thereby lost much of their spin polarization (see table 3.1).

An intriguing situation occurs also when studying the Fe_{v_v}Co and Mn_{v_v}Co structures of chapter 4 with the Co-ended tip (fig. 5.11). In either case at strong fields it is the peak at negative tip-voltage that is highest, as we saw for the

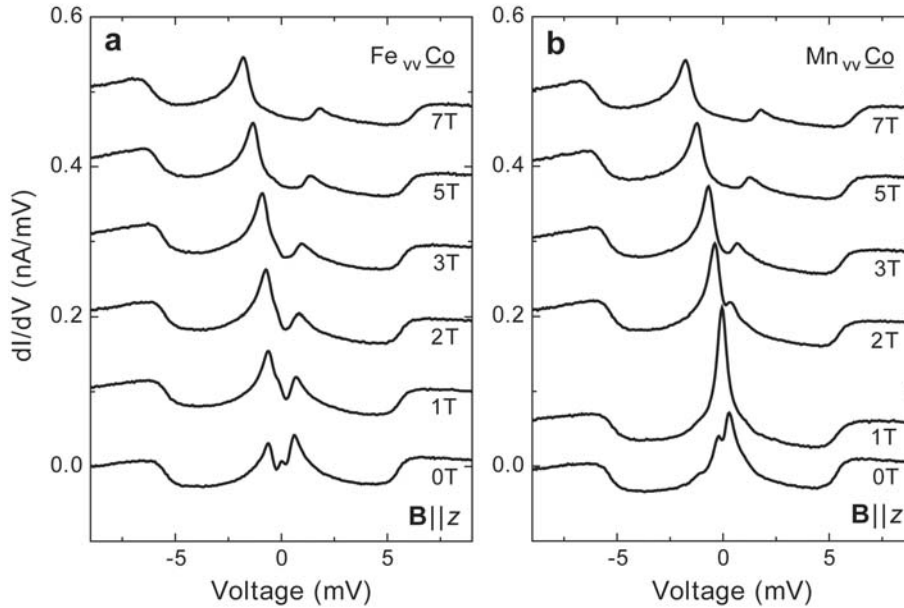


Figure 5.11: dI/dV -spectra measured over the Co atoms of $\text{Fe}_{\text{vv}}\text{Co}$ (a) and $\text{Mn}_{\text{vv}}\text{Co}$ (b) at various fields oriented along z (i.e. out-of-plane). The measurements were performed with the same Co-ended tip as used in fig. 5.9. Although this tip significantly alters the peak heights, their positions as well as those of the steps (being used for analysis in chapter 4) are not expected to be influenced by it. All non-zero field spectra are shifted for clarity.

single Co atom. But at low field strengths, e.g. in case of $\text{Mn}_{\text{vv}}\text{Co}$ below the point where the ground state changes to antiparallel around 1 T, suddenly the positive-voltage peak becomes dominant: the Co spin has flipped around.

The anomalous spectroscopic asymmetry presented in this section was occasionally encountered also when other magnetic atoms (Mn or Fe) were picked up instead of Co. In one instance it even was the neutral tip (i.e. with a Cu atom) that showed this behavior, albeit weaker, while the same tip with a Co atom produced symmetric spectra. This might have been caused by a second magnetic atom being incorporated in the tip structure close to the apex, such that its effects were cancelled when another magnetic atom was picked up.

All these tips could prove to be highly valuable spin filters, in the sense that the filtering aspect can be switched on or off simply by replacing the last atom. However, one thing we haven't considered at all is the question how strongly they are magnetized. A spin-polarized tip is hardly useful if the least stray field induced by the sample below it would reverse its filter. In order to answer this question, we should basically repeat the kind of experiments discussed in chapter 3 – to determine the magnetic anisotropy energies of an atomic spin in a certain environment – with the roles of tip and sample inverted.

5.4 Closing Remarks

The preliminary findings presented in this chapter demonstrate how we have only barely begun exploring the richness of this fascinating experimental system. Clearly spin excitation spectroscopy is a fantastic tool and Cu_2N an almost perfect study object to use it on. Among the countless parameters that one can tune during further experiments are the length and direction of the vector separating coupled spins, as well as the size, geometry and composition of larger spin structures. Additionally several other d -shell magnetic elements such as Ti, Cr and Ni can be studied to verify or expand our hypotheses on magnetic anisotropy and Kondo-screening for various values of S .

But why limit ourselves to Cu_2N ? There are bound to be numerous other surfaces just as useful for performing spin excitation spectroscopy experiments. While the square lattice of Cu_2N was found to be exquisite for anisotropy measurements, surfaces with a threefold symmetry such as triangular or hexagonal lattices might be ideal for building circular spin chains. Especially when antiferromagnetic rings can be constructed that contain an odd number of atoms, all sorts of spin frustration effects might be observed.

From a technological viewpoint it may be worthwhile to search for surfaces that present an even stronger magnetic anisotropy, allowing stable atomic bits to be realized at higher temperatures. In this respect it is important to understand as much as possible of the surface molecular network of Cu_2N and the impact it has on the orientation of atomic spins incorporated into the network, as well as its possibilities for coupling spins ferromagnetically.

The concept *spectroscopy* is used very widely throughout experimental physics. Auger spectroscopy, NMR spectroscopy, Raman spectroscopy and spectroscopy of visible and UV light absorption by atoms are only a few of the many examples. While their underlying mechanisms are quite different, all these techniques are based on the same general principle: to characterize a system by observing not only in what state it happens to be, but also what excitations can be made to it. With the developments of inelastic electron tunneling spectroscopy and spin excitation spectroscopy, similar characterization can now be performed in combination with the fabulous spatial resolution that only an STM can provide.

